Nano Today 35 (2020) 100965

Contents lists available at ScienceDirect

Nano Today

journal homepage: www.elsevier.com/locate/nanotoday

Multifunctional bioreactive-nanoconstructs for sensitive and accurate MRI of cerebrospinal fluid pathology and intervention of Alzheimer's disease

Chunsheng He[a,1], Taksim Ahmed[a,1], Azhar Z. Abbasi[a,1], Lily Yi Li[a], Warren D. Foltz[b], Ping Cai[a], Erin Knock[c,2], Paul E. Fraser[c], Andrew M. Rauth[d], Jeffrey T. Henderson[a], Xiao Yu Wu[a,*]

[a] Leslie Dan Faculty of Pharmacy, University of Toronto, 144 College Street, Toronto, Ontario, M5S 3M2, Canada
[b] STTARR Innovation Centre, Department of Radiation Oncology, Princess Margaret Hospital, Toronto, Ontario, M5G 2M9, Canada
[c] Tanz Centre for Research in Neurodegenerative Diseases, Department of Medical Biophysics, University of Toronto, Toronto, Ontario, M5T 2S8, Canada
[d] Departments of Medical Biophysics and Radiation Oncology, University of Toronto, Princess Margaret Cancer Centre, 610 University Avenue, Toronto, Ontario, M5G 2M9, Canada

ARTICLE INFO

Article history:
Received 25 March 2020
Received in revised form 5 August 2020
Accepted 25 August 2020
Available online 11 October 2020

Keywords:
Bioreactive nanoconstruct
Alzheimer's disease
Cerebrospinal fluid pathology
MRI
Early-stage diagnosis and intervention

ABSTRACT

Lack of sensitive detection of early onset and progression of Alzheimer's disease (AD) by non-invasive methods limits the development and implementation of therapeutic interventions. Given that cerebral oxidative stress and inflammation occur before diagnosable clinical symptoms, a multifunctional theranostic nanoconstruct (NC) system has been developed. It gains entry to the brain by a targeting moiety, binds selectively with soluble amyloid-β (Aβ) and Aβ plagues *via* a conjugated anti-Aβ antibody. The NC is activated by endogenous reactive oxygen species (ROS), enhancing magnetic resonance (MR) contrast signals in disease-affected areas. It exhibits superior performance in detecting cerebrospinal fluid (CSF) pathology in an AD mouse model by MR imaging. Intravenously injected NCs significantly amplify T1-weighted MR signals in the CSF by 1.51–2.24 fold, nearly proportional to cerebral concentrations of ROS and pro-inflammatory cytokine interleukin-1β (IL-1β). The NC-enhanced CSF MR signals demonstrate high detection sensitivity (88.9 %) and specificity (100 %) even at early-stage AD. Moreover, the NCs protected primary cortical neurons from oxidative stress *in vitro* and reduce cerebral ROS and IL-1β levels in AD mice by 36 %–83 %. This multifunctional NC-based technology may allow for early detection and treatment of AD prior to cognitive decline when therapies may prove more beneficial.

Introduction

Alzheimer's disease (AD) is the most common cause of dementia affecting 40–50 million people worldwide, including ~5.8 million Americans [1]. Unfortunately the standard of care treatments for AD only manage symptoms, and currently there is no curative or approved disease-modifying therapeutics for AD [2,3]. Despite tremendous efforts and expenditures so far, most clinical trials over the past decades have failed to achieve meaningful clinical benefits for AD [1,3–6]. Many contributing factors to such failures have been postulated to include variable origins and rates of disease progression, inappropriate therapeutic targets and patient selection, late intervention, and suboptimal dosing [1,2,4,7]. Moreover, presence of the blood-brain barrier (BBB) limits efficient transport of therapeutic agents into neocortex and deeper structures [3,5,8]. The late intervention of the disease is largely due to the lack of a sensitive and accurate detection method for early stage AD [6,9]. Neurobiological changes in AD can occur much earlier than the cognitive decline diagnosed by clinical methods. For example, changes in cerebrospinal fluid (CSF) biomarkers, *e.g.* hyperphosphorylated tau (p-tau) and amyloid β-42 (Aβ42) occur 15–20 years prior to the clinical onset of AD [10,11]. However, clinical diagnosis of AD is conducted in accordance with exclusion criteria by clinical symptoms (*e.g.* impaired memory and cognitive function) [1,10,12]. The diagnostic sensitivity and specificity of these methods are relatively low and are only definitive when identifying AD at its irreversible

* Corresponding author.
E-mail address: sxy.wu@utoronto.ca (X.Y. Wu).
[1] These authors contributed equally.
[2] Current address: STEMCELL Technologies Inc., 570 West Seventh Avenue, Vancouver, BC, V5Z 1B3, Canada.

https://doi.org/10.1016/j.nantod.2020.100965
1748-0132/

stages [2,10,12,13]. Therefore, for early detection and complementary imaging-based diagnosis of AD, fluid biomarkers (*e.g.* CSF Aβ42 and p-tau) are measured. However CSF sampling is labor intensive, costly, and invasive; it requires lumbar puncture at L3-L5 which carries some risk of CNS injury infection. Therefore analysis of CSF biomarkers by this method is not broadly practiced clinically [10,11].

Various imaging techniques have been applied to detect AD non-invasively including positron emission tomography (PET), PET/computed tomography (CT), single-photon emission computed tomography (SPECT) scans and magnetic resonance imaging (MRI) [14–16]. PET scan measures metabolic changes using radiolabeled fluorodeoxyglucose ([^{18}F] FDG), or Aβ plaques by amyloid tracers such as Pittsburgh Compound-B (PiB). However, PET scan requires use of expensive radioactive probes of limited availability [15,17]. In addition, high levels of Aβ plaques found in later stages of AD may not correlate well with AD dementia [17,18]. By contrast MRI is a powerful tool for clinical assessment of patients with suspected AD by measuring the volume and structural changes in the brain [15,19]. Structural MRI can determine atrophy of medial temporal lobe, hippocampal, entorhinal cortex and subiculum, as potential early indicators of future AD dementia risk [20,21].

To enhance MRI signal, gadolinium (Gd) based contrast agents are commonly used clinically. However application of Gd-based contrast agents have been linked to significant nephrogenic systemic fibrosis in some patients, particularly those with severe renal dysfunction [22]. Studies have also shown deposition of Gd in the brain and bones can occur over an extended periods [23,24]. Moreover the majority of current MRI contrast agents possess poor selectivity and limited ability to penetrate the BBB for early and accurate detection of CNS/CSF biomarkers in AD [5,8,25,26].

Increasing evidence has shown that early events in AD are associated with hypoxia and oxidative stress [27,28]. Neuropathology such as neuro-inflammation induced by reactive oxygen species (ROS), *e.g.* H_2O_2, reportedly occur prior to overt amyloid plaque accumulation and cognitive AD progression [29]. In addition, ROS, Aβ oligomers and fibrils are known to activate microglia and astrocytes triggering the secretion of pro-inflammatory cytokines that promote disease progression [30]. To circumvent ROS-induced AD progression, various antioxidants and anti-inflammatory drugs have been investigated [31], but with limited success [1,5,8,32].

In light of early signs of oxidative stress, inflammation and neurotoxicity of soluble Aβ oligomers in AD brains, we developed an anti-Aβ antibody (aAβ)-conjugated, brain-targeted (BT), and ROS-activatable (RA) MnO_2 nanoparticle (MnO_2-NPs)-containing nanoconstruct (NC) (aAβ-BTRA-NC) (Fig. 1a). The multifunctional aAβ-BTRA-NCs can effectively cross the BBB, selectively accumulate in Aβ- and ROS-affected brain tissue (Fig. 1b), react with or break down endogenous H_2O_2 to produce O_2 [33,34], and release paramagnetic manganese ions (Mn^{2+}) *in situ* enhancing local MRI contrast (Fig. 1c). Meantime, the multifunctional polymer can simultaneously bind with soluble Aβ oligomers or Aβ plaques *via* the conjugated aAβ and complex with free Mn^{2+} ions *via* the carboxylic groups, thereby enhancing MRI contrast in relation to the level and location of ROS and Aβ pertinent to disease stage (Fig. 1c). Owing to the consumption of H_2O_2 and production of O_2, the aAβ-BTRA-NC is expected to reduce local oxidative stress and hypoxia that are detrimental to neurons.

Materials and methods

Synthesis of BTRA-NCs and aAβ-BTRA-NCs

A brain targeted polymer (BTP) was synthesized by grafting polymerization of poly(methacrylic acid) and polysorbate 80 (PS 80) onto starch [35]. Anti-Aβ antibody 4G8 conjugated-BTP (aAβ-BTP) was prepared by EDC/ N-hydroxysuccinimide (NHS) coupling of 4G8 with the BTP. Briefly, 500 mg of purified BTP, 100 mg of EDC, and 100 mg of NHS were dissolved in 10 mL of distilled de-ionized water (DDIW, Milli-Q water, MilliPore Canada Ltd, Etobicoke, ON, CA) and allowed to react for 2 h at room temperature. Antibody (4G8) solution (100 μL, 20 mg mL-1, PBS, pH 7.4) was added to the activated BTP solution and allowed to react at 37 °C for 24 h. The product solution was neutralized to pH 7.4 using 0.1 N NaOH, and purified by extensive re-suspending and filtered by Nanosep® 300 K Omega centrifuge filters (Sigma-Aldrich, Canada). The purified product was then lyophilized and stored in a desiccator at 4 °C. Brain targeted and ROS activatable nanoconstructs (BTRA-NCs) and anti-Aβ (aAβ)-BTRA-NCs were prepared using a facile "one-pot" synthesis method shown schematically in Fig. 1a. Briefly, 100 μL of $KMnO_4$ in DDIW (4.8 w/v%) and 220 μL of poly(vinyl alcohol) (PVA) in DDIW (0.5 wt%) were mixed in a 15 mL conical tube and heated to 52 °C for 4 min to produce small precursor MnO_2. Then ethyl arachidate (15 mg) was added and stirred for another 4 min to form a crude emulsion, to which 15 mg of BTP (or 16 mg of 4G8-BTP) dissolved into 200 μL of DDIW was introduced. The mixture was sonicated for 3 min using a Hielscher UP 100H probe ultrasonicator (Ringwood, NJ, USA) at 80 % peak amplitude. The resultant nanoemulsion was then quickly transferred into dextrose solution (5 wt%) being stirred on ice and topped up to 1 mL. The produced NC emulsion was then purified by extensive re-suspending and filtered by Nanosep® 100 K Omega centrifuge filters (Mississauga, ON, CA). The completion of $KMnO_4$ conversion to MnO_2-NPs and self-assembly into the PVA-lipid matrix-BTP was confirmed by ultraviolet-visible (UV–vis) spectrophotometry analysis (Supplementary Information (SI), Fig. S1a) and XPS (X-ray photoelectron spectroscopy), Figs. 2b & SI, S1b). The final concentration of MnO_2 in the suspension was determined to be 30 mM *via* inductive coupled plasma atomic emission spectroscopy (ICP-AES, Optima 7300 DV ICP-AES, PerkinElmer Ltd, Boston, MA, USA) analysis. The produced suspensions were stored at 4 °C and further diluted with cell medium or sterile saline for *in vitro* and *in vivo* studies, respectively.

MR imaging of brains of AD mice of various ages and age-matched wild-type mice

In vivo MRI of mouse brains were performed using a 7 T micro-MRI (BioSpec USR, Bruker, Ettlingen, DE) equipped with the B-GA12 gradient coil, 7.2 cm inner diameter linearly polarized cylindrical volume coil for radiofrequency (RF) transmission, and a dedicated murine brain receive-only RF coil for MR signal reception. Mice were anesthetized by breathing 1.8 % isoflurane and imaged in prone position on a custom slider bed. A pneumatic pillow fixed above the thorax/abdomen provided a signal for respiratory monitoring (SA Instruments, Stony Brook, NY, USA). Mice were also prepared *via* tail vein cannulation with a 27 G needle and a precision line to enable automated contrast agent injection following mouse positioning at system isocenter (Harvard Apparatus, Holliston, MA, USA). At baseline and at time-points of approximately 0, 30, 60, 90, and 120 min post-injection, high resolution 3D T1-weighted image sets were acquired without moving the mouse (3D-FLASH, TE/TR = 4.5/75 ms, 320 × 320 × 40 matrix over a 19.2 × 19.2 × 10 mm field-of-view for 60 × 60 × 250 μm spatial resolution; 75 kHz readout bandwidth; 32 min acquisition time). Quantitative measurements were performed in registered manually-segmented brain cortex, hippocampus and CSF regions-of-interest (ROIs), using MIPAV software (National Institutes of Health, Bethesda, MD).

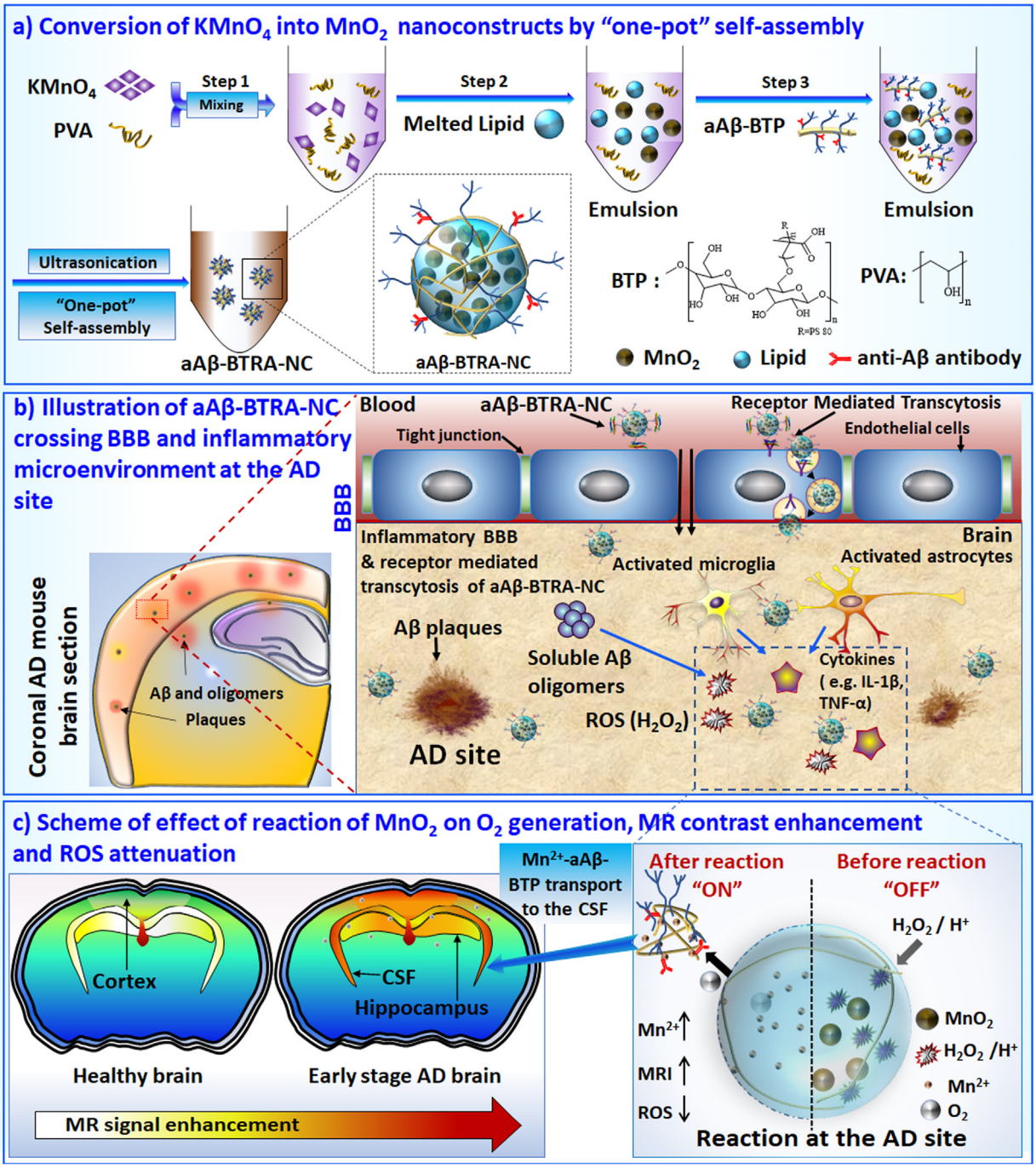

Fig. 1. a) Schematic diagram depicting the process of conversion of $KMnO_4$ into MnO_2-contaning nanoconstruct by self-assembly using BTP and lipid in "one-pot". **b)** Schematic illustration of the BBB-crossing mechanisms of aAβ-BTRA-NCs in healthy and AD brain and inflammatory microenvironment of AD site where there exist elevated levels of ROS (*e.g.* H_2O_2) and inflammatory cytokines (*e.g.* IL-1β and TNF-α). In healthy brain, the NCs cross the BBB *via* transcytosis mediated by low density lipoprotein receptor (LDLR). In the inflammatory AD brain, the NCs can also enter brain parenchyma *via* leaky vessels. **c)** Schematic diagram showing the effect of MnO_2 carried by aAβ-BTRA-NCs on O_2 generation, MRI contrast enhancement and ROS attenuation. The aAβ-BTRA-NCs accumulate at Aβ plaque area and react with the ROS (*e.g.* H_2O_2), generating Mn^{2+} ions locally. The multifunctional aAβ-BTP can bind with soluble Mn^{2+} and Aβ oligomers in the CSF or transport them to CSF from other areas. IL-1β: Interleukin 1 beta; TNF-α: tumor necrosis factor-alpha.

Results and discussion

The novel multifunctional polymer-lipid-inorganic hybrid NC (*i.e.*, BTRA-NC) were prepared using a facile and easily scaled-up "one-pot" synthesis method. The inorganic MnO_2-NPs were generated by reducing $KMnO_4$ with PVA in an aqueous medium, to which melted lipid was introduced to form a MnO_2-NPs-lipid crude emulsion. The hydrophobic interaction between BTP and the lipid domain led to the formation of the NCs upon cooling with a monolithic-matrix structure by self-assembly (Figs. 1a, S1). The polysorbate 80 (PS80) in BTP protrudes outward stabilizing the NCs in plasma and facilitating BBB-penetration (Fig. 1b). To target soluble Aβ oligomers and Aβ plaques, BTP is functionalized with anti-Aβ antibody at a 3.3 wt % grafting ratio to the polymer (SI). UV–vis spectroscopy and XPS confirmed PVA converted $KMnO_4$ to MnO_2 (Figs. 2b and S1a–b). The resultant BTRA-NCs and aAβ-BTRA-NCs were 66–69 nm in diameter, with polydispersity indices (PDI) of 0.26–0.27, and zeta potential of approximately −50 mV (Figs. 2a,

Formulations	Size (d, nm)	Polydispersity Index (PDI)	ζ-Potential (mv)	R_1 Relaxivity (mM sec)$^{-1}$	
				Without H_2O_2	With H_2O_2
BTRA-NC	65.9 ± 5.2	0.26 ± 0.02	-50 ± 3.8	2.9 ± 0.8	16.6 ± 1.2
aAβ-BTRA-NC	68.6 ± 1.8	0.27 ± 0.02	-49 ± 4.1	3.0 ± 0.5	16.7 ± 0.9

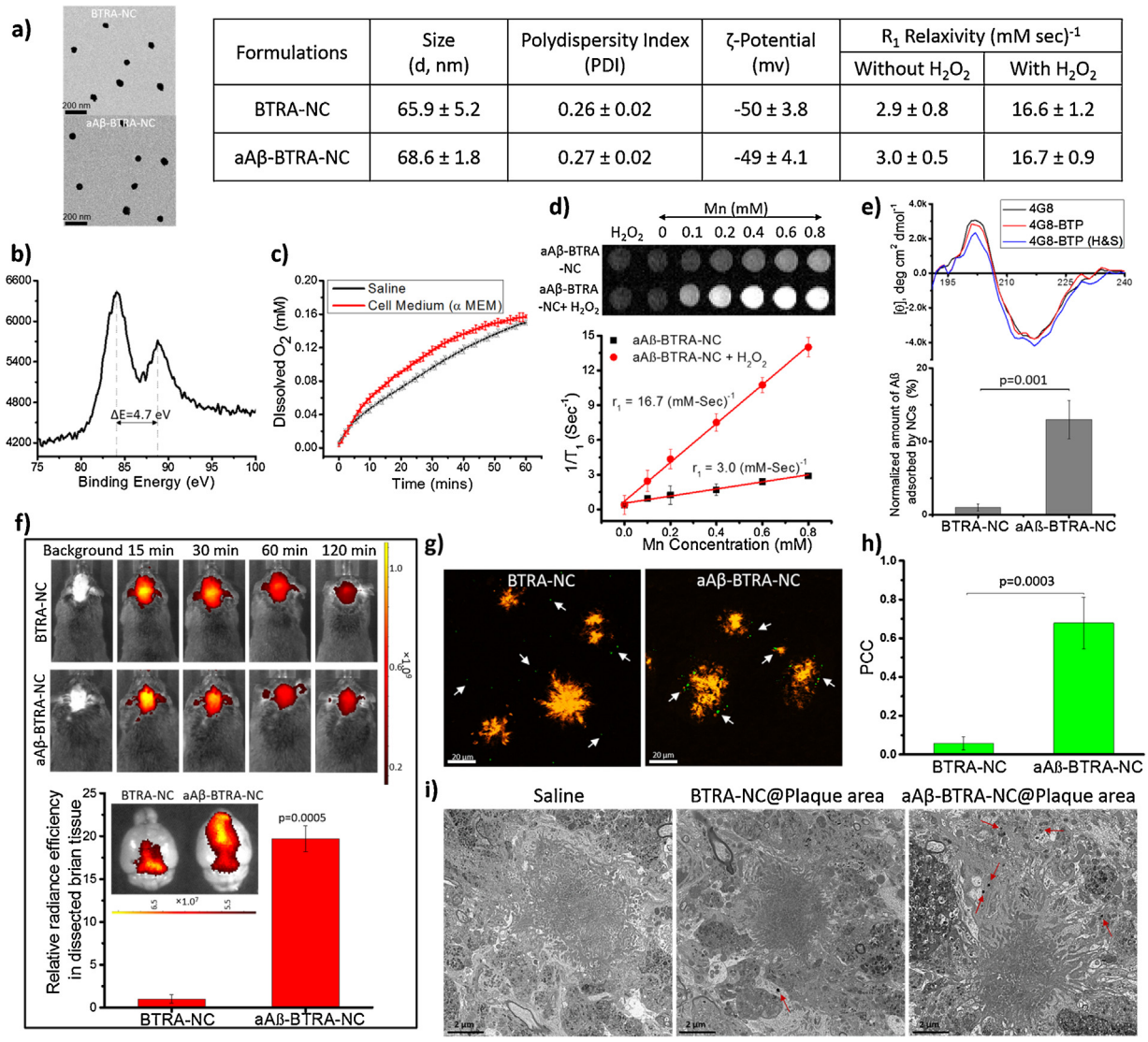

Fig. 2. **a)** Summary of particle size, PDI, Zeta potential, representative TEM images and relaxivity (r1) of NCs. **b)** XPS Mn3s spectra of BTRA-NCs. **c)** O_2 generation by addition of H_2O_2 to aAβ-BTRA-NCs suspensions in saline or growth medium. **d)** Top: Representative T_1-wt MR images of aAβ-BTRA-NCs alone, or aAβ-BTRA-NCs+H_2O_2 (500 μM) at 7 T. Bottom: Relaxation rate $1/T_1$ *vs*. Mn concentration plots. **e)** Top: CD spectra of aAβ, aAβ-BTP and aAβ-BTP after heating and sonication (aAβ-BTP H&S). Bottom: Percent of soluble Aβ1-42 peptide adsorbed by BTRA-NCs and aAβ-BTRA-NCs. **f)** Top: Representative *in vivo* optical images of TgCRND8 mouse following i.v. injection of NCs at various time points. Bottom: *Ex vivo* brain images and quantitative results for fluorescent intensity recorded at 120 min post treatment. **g)** CLSM images of brain sections from Tg mouse at 120 min post treatment. Aβ plaques are shown as orange; and NCs (green) (white arrow indicates the NCs). **h)** Degree of co-localization of NCs and Aβ plaques determined by Pearson's correlation coefficient (PCC). **i)** TEM images of Tg mouse brain sections at 120 min post NCs treatment. Red arrows show the accumulation of NCs around plaque areas. Scale bars =2 μm. All results are expressed as mean ± standard deviation (SD) (n = 3).

S2a–b). Transmission electron micrographs (TEM) portrayed NCs in uniform spherical shape (Fig. 2a). The NCs were stable for over 48 h at 37 °C in 50 % fetal bovine serum (FBS) (Fig. S2c–e). The reactivity of NCs towards H_2O_2 to generate O_2 was confirmed in both saline and cell culture media (Fig. 2c). *In vitro* MRI showed 5.6–5.7-fold increase in T_1 relaxivity (r1) in the presence of H_2O_2 due to the conversion of MnO_2 to paramagnetic Mn^{2+} ions (Figs. 2d, S2f–g). Both BTRA-NCs and aAβ-BTRA-NCs showed 3.5-fold higher r1 values (16.6 – 16.7 mM^{-1} sec^{-1}, Figs. 2a & d, S2g) compared to the commercially available gadolinium (Gd) based MR contrast agent, GADOVIST® 1.0 (4.7 mM^{-1}-sec^{-1}).

Far UV circular dichroism (CD) spectra of purified aAβ-BTP in solution with or without exposure to NC synthesis conditions (heat and sonication, H&S) were identical to that of freshly prepared solution of aAβ antibody (Fig. 2e). These results suggest that the secondary structure of aAβ was well preserved during the chemical reaction and NC preparation. A strong binding of aAβ-BTRA-NCs with soluble Aβ was demonstrated by an absorption test which showed >10-fold of Aβ1-42 peptide removed from the medium by aAβ-BTRA-NCs than the non-targeted BTRA-NCs (Fig. 2e).

The effect of aAβ conjugation on NC-crossing the BBB was evaluated using an *in vitro* 3D-human BBB model assay. Cyanine 5.5 (Cy5.5)-labeled BTRA-NCs or aAβ-BTRA-NCs were introduced to the apical side of the transwell and fluorescence intensity in the medium on the basolateral side was measured using fluorescence spectroscopy. Both BTRA-NCs and aAβ-BTRA-NCs permeated >10 % of the administered dose after 30 min (Fig. S2h), indicating that aAβ conjugation did not adversely affect BBB-crossing capability of the NCs. The binding affinity of aAβ-BTRA-NCs with Aβ after *in vitro* BBB-crossing test was confirmed by incubating aAβ-BTRA-NCs collected from the basolateral side of the transwell with Tg mouse brain cryo-sections. Co-localization of aAβ antibody staining (green), Cy5.5 labeled aAβ-BTP or aAβ-BTRA-NCs (red) with Aβ plaques (resorufin staining, orange) for all formulations was shown

by confocal laser scanning microscopy (CLSM) of brain tissue slices (Fig. S2i).

Nanocarrier based receptor-targeting approaches have shown potential in delivering therapeutic agents across the BBB [5,26,36–38]. It has been reported that adsorption of apolipoprotein E (ApoE) from the plasma onto the surface of NPs facilitated their BBB-crossing *via* low density lipoprotein (LDL) receptor-mediated transcytosis [38–44]. To test the hypothesis that ApoE decoration is critical for NCs to cross the BBB (Fig. 3a), we first confirmed adsorption of ApoE onto BTRA-NCs using sodium dodecyl-sulfate polyacrylamide gel electrophoresis (SDS-PAGE) (Fig. S3). We then investigated extravasation of the BBB-impermeable dye Hoechst 33342 and fluorescein isothiocyanate (FITC)-labeled BTRA-NCs. The BTRA-NCs with or without incubation with ApoE (BTRA-NC (+/-) ApoE) were injected intravenously (i.v.) into ApoE knockout (KO) mice, while BTRA-NCs without ApoE treatment were injected into normal C57BI6J mice (Fig. 3). The CLSM images of brain tissue sections showed that the BTRA-NCs without ApoE incubation (Dye-NC(-)ApoE) stained parenchymal cell nuclei (blue) in normal mice, while only ApoE treated BTRA-NCs (Dye-NC(+)ApoE) could stain the cells in the ApoE-KO mouse brain (top two panels, Fig. 3b). In these panels labeled nuclei were identified as distal to local blood vasculature (identified *via* Texas Red-dextran infusion) and FITC-NCs in the brain tissue were outside of blood vessels (green, Fig. 3b). In contrast untreated BTRA-NCs (Dye-NC(-)ApoE) or free ApoE plus free dye remained confined within blood vessels as evidenced by co-localization of blue (nuclei) and red (blood vessels) staining and an absence of blue nuclei in the brain parenchyma of ApoE-KO mice (Fig. 3b). Quantification of FITC and dye positive labeling outside of brain blood vessels further confirmed significantly higher BBB-penetration and extravasation of BTRA-NCs with ApoE than without NP constructs lacking ApoE in ApoE-KO mice (Fig. 3c, d). These results demonstrate that the BTRA-NCs are able to extravasate from brain microvasculature to deliver a BBB-impermeable agent into the CNS. The results further verify that BTRA-NCs cross the BBB through a mechanism that involves adsorption of ApoE from plasma and receptor-mediated transcytosis through brain vascular endothelial cells across the intact BBB [39,40,43,44].

The selective targeting of aAβ-BTRA-NCs in AD brains and Aβ plaques was evaluated by *in vivo* and *ex vivo* fluorescence imaging and CLSM as compared to BTRA-NCs in six-month old TgCRND8 AD (Tg) mice, a murine model for AD [45]. Much higher accumulation and retention of aAβ-BTRA-NCs in the AD brains were found (Figs. 2f–h, S4a–b), with 10-fold higher fluorescence intensity in the brain tissue 120 min following treatment than BTRA-NCs (Fig. 2f). The CLSM of *ex vivo* brain sections revealed that more FITC-aAβ-BTRA-NCs (green) accumulated within Aβ plaque regions (orange), or with closer proximity than FITC-BTRA-NCs (Fig. 2g). Pearson's correlation coefficient (PCC) of green (NCs) and orange (Aβ plaques) pixels was found to be 0.65 for aAβ-BTRA-NCs and 0.1 for BTRA-NCs, respectively (Fig. 2h), demonstrating the ability of aAβ-BTRA-NCs to target Aβ plaques. TEM images further confirmed more aAβ-BTRA-NCs (black dots) than BTRA-NCs accumulated within Aβ plaque regions in the AD brain tissue (Fig. 2i). Immuno-histochemical (ICH) analysis of the hippocampus region of Tg mouse brain revealed a deposition of aAβ from the aAβ-BTRA-NCs in brain parenchyma outside of blood vessels (Fig. S4c). These results verified that the anti-Aβ antibody retained bioactivity *in vivo* and enabled selective accumulation of aAβ-BTRA-NCs in Aβ-rich brain tissue.

The potential of aAβ-BTRA-NCs for non-invasive MRI detection of early stage and progression of AD was assessed using 3-, 6- or 9-month old Tg mice or age-matched wild-type (WT) littermates. MRI scans were performed prior to treatment (baseline) and at 30, 60 and 120 min after i.v. administration of aAβ-BTRA-NCs. MRI signals acquired as early as 30 min post aAβ-BTRA-NC injection were significantly enhanced in CSF, cortex and hippocampus of Tg mice. In contrast, the commercially available Gd-based contrast agent GADOVIST® 1.0 produced minimal signal enhancement at the same dose (Fig. S5).

The T_1-wt MR signals in the regions of cortex, hippocampus, and CSF were normalized against their own baselines and plotted as a function of mouse age and time post NC injection (Fig. S6a–d). Little change in the signals was observed with time and age in WT mice, while signal enhancement in Tg mice was detected as early as 3-months of age and increased with mouse age, indicating greater disease severity (Fig. S6a–d). In hematoxylin and eosin (H & E) stained brain sections with labeled Aβ plaques (brown dots), the plaques could hardly be visualized in the 3-month old Tg mouse brain, while their density profoundly increased at 6- and 9-months of age (Fig. 4 a). This result is consistent with a previous report on age-dependent amyloid deposition in Tg mice that Aβ42 content increased ~70-fold from 115 to 728 ng/g of brain at 2.5 months to 12,476–29,260 ng/g of brain at 6.5 months of age [46].

The T_1-wt signal enhancement in the cortex and hippocampus area exhibited a strong dependence on the post NC-injection time, while the signal in the CSF was nearly independent of the time from 30 min to 120 min (Fig. S6a–d). The gradual increase in the signal in cortex and hippocampus areas may be due to slow penetration of NCs through the brain tissue and conversion of MnO_2 into Mn^{2+} ions. In contrast, the rapid appearance of a strong signal in the CSF may suggest easier transport of NCs and greater availability of ROS and Aβ oligomers in the CSF compared to other areas. Moreover, dissolved aAβ-BTP with capability of binding both Aβ oligomers through the antibody and Mn^{2+} *via* poly(methacrylic acid) chains in the BTP, as confirmed by differential pulse voltammetry (Fig. S7), could magnify the MRI signal in CSF where soluble Aβ oligomers exist. The dual binding affinity of aAβ-BTP can also reduce free Mn^{2+} ions and soluble Aβ levels in the brain and CSF, diminishing their toxic effects [33].

To balance the cost of imaging preparation time and sufficient MRI signal enhancement, images acquired 60 min after injection of aAβ-BTRA-NCs were selected for further analysis. The normalized T_1-wt signal enhancement in CSF was the strongest among three investigated areas, increasing >1.5-fold (1.51, 1.65, and 2.24 for 3-, 6- and 9-months of age, respectively) from the baseline, while only 1.05–1.16/1.21-fold increases were found in hippocampus and cortex areas (Fig. 4c–e). The enhanced signals in the CSF for all age groups were significantly different from those in the WT mice ($p = 1 \times 10^{-5}$–4×10^{-7}); the differences were statistically significant between 6-months and 9-months of age ($p = 0.005$) and between 3-months and 9-months of age ($p = 0.0003$) (Fig. 4c). In contrast, statistically different signal enhancement in the cortex and hippocampus was only found between 9-month old Tg mice and WT mice ($p = 0.003$) (Fig. 4d–e). These results demonstrate that non-invasive MRI of CSF pathology enabled by aAβ-BTRA-NCs has the potential to determine different stages of AD pathology.

The data acquired at 60 min post injection were further used to calculate diagnostic sensitivity (true positive rate) and specificity (true negative rate) [47]. As summarized in Fig. 4f, the MR signal enhancement in CSF exhibited the highest diagnostic sensitivity (88.9 %, 95 % CI) in Tg mice and specificity (100 %, 95 % CI) in WT mice regardless of mouse age, followed by those in hippocampus (sensitivity 85.7 %–88.9 %; selectivity 77.8 %–100 %) and cortex (sensitivity 83.3 %–87.5 %; selectivity 70.0 %–87.5 %) increasing with mouse age. The lowered sensitivity and selectivity for hippocampus and cortex may also be related to the slow penetration of NCs through the brain tissue and conversion of MnO_2 into Mn^{2+} ions with the gradual increase in signals, resulting in a lower signal-to-noise ratio. We postulate that once NCs reach inflammatory regions of brain, the reaction of ROS with NCs together with their metabolic

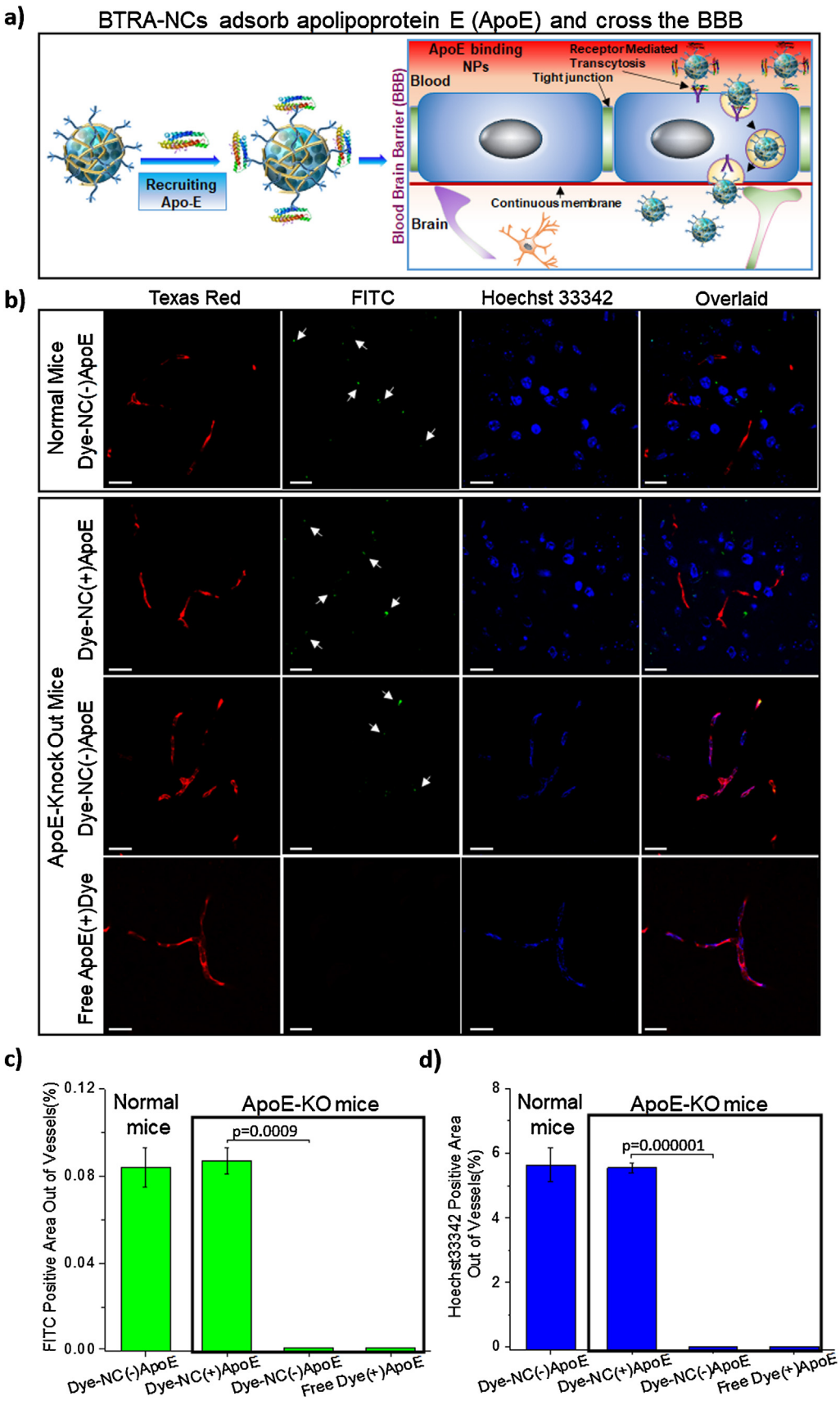

Fig. 3. **a)** Schematic diagram depicting BTRA-NCs with recruited apolipoprotein E facilitating LDLR-mediated BTRA-NC across the BBB. **b)** CLSM images of healthy C57BL6j and ApoE-Knockout (KO) mouse brain sections following the treatment with different formulations (Y-axis legend). Two hours post i.v. injection of the formulations, blood vessels were labeled by i.v. administration of Texas Red-dextran 15 min before euthanasia. Hoechst 33342 dye-labeled cell nuclei appear blue. Texas Red-dextran and FITC appears as red and green, respectively. Arrows indicate representative FITC-labeled NCs. Scale bar corresponds to 20 μm for all images. **c)** Quantification of FITC-labeled NCs and **d)** Quantification of Hoechst 33342 positive areas outside of blood vessels. Fifteen stacks from 3 mice were examined. p values indicate statistically significant difference as compared to Dye-NC(-)ApoE treated groups. Error bars indicate the standard deviation of three independent experiments (n = 3).

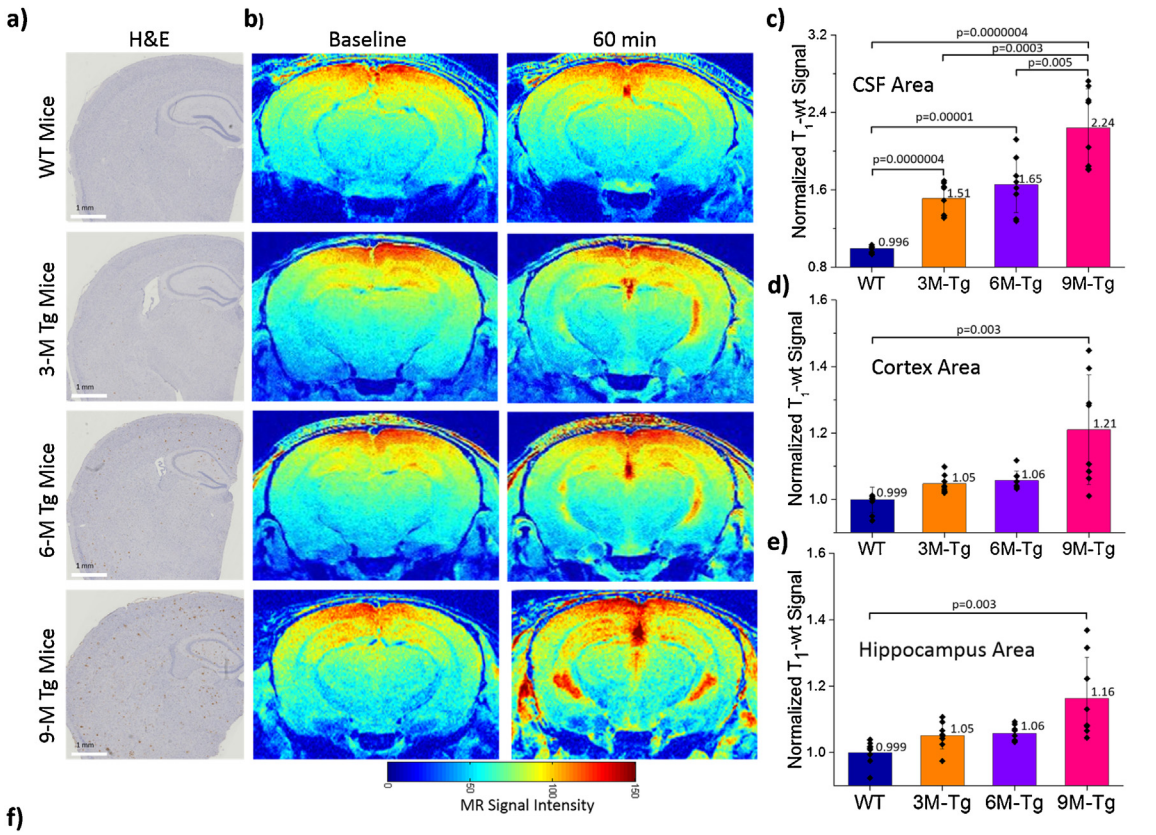

f)

Area	Sensitivity % (95% CI)			Specificity % (95% CI)		
	3-M	6-M	9-M	3-M	6-M	9-M
CSF	88.9 (51.8-99.7)	88.9 (51.8-99.7)	88.9 (51.8-99.7)	100 (59.0-100)	100 (59.0-100)	100 (59.0-100)
Hippocampus	85.7 (42.1-99.6)	85.7 (42.1-99.6)	88.9 (51.8-99.7)	77.8 (40.0-97.2)	77.8 (40.0-97.2)	100 (59.0-100)
Cortex	83.3 (35.9-99.6)	87.5 (47.4-99.7)	87.5 (47.4-99.7)	70.0 (34.6-93.3)	87.5 (47.4-99.7)	87.5 (47.4-99.7)

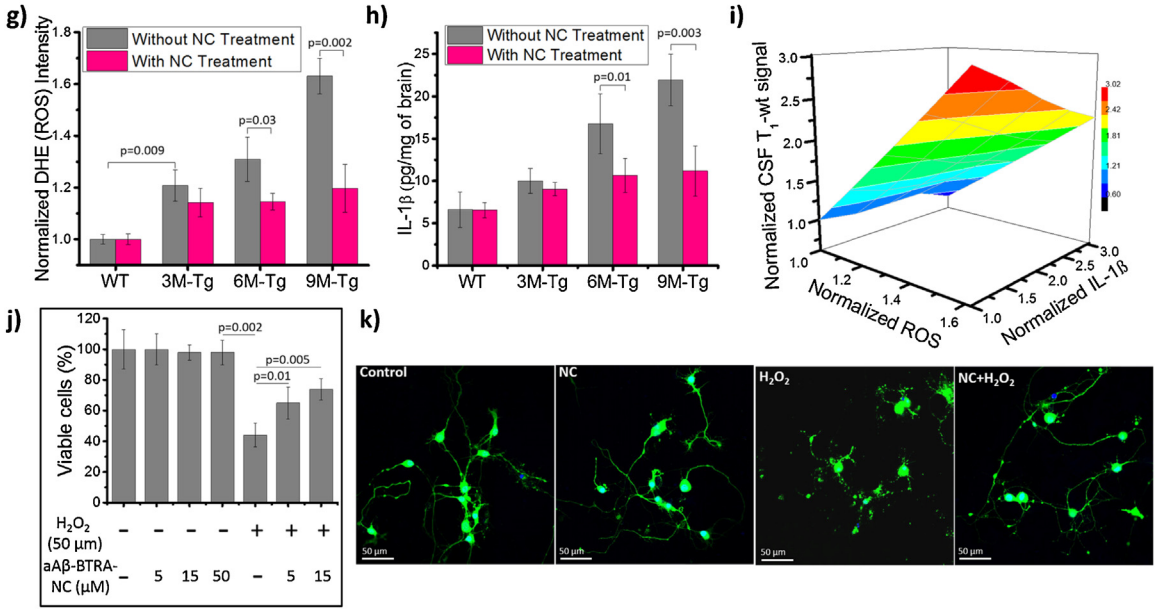

Fig. 4. **a)** H&E staining of typical brain sections of WT mice and Tg mice of different ages (3-, 6-, and 9-months). **b)** Representative *in vivo* T1-wt MR images of brains of WT mice and Tg mice of different ages acquired before (baseline) or 60 min after aAβ-BTRA-NC treatment. **c-e)** T_1-wt MR signal enhancement relative to baseline in different brain regions at 60 min post-injection (**c:** CSF, **d:** cortex, **e:** hippocampus regions) for Tg mice at different ages. WT littermates at different ages were combined into one group due to the minimal and similar MR contrast enhancement after aAβ-BTRA-NC treatment. Data are presented as mean ± SD (n = 8). **f)** Diagnostic sensitivity and specificity by aAβ-BTRA-NC-enhanced MR signals for Tg mice (95 % CI: 95 % confidence interval). **g)** ROS levels indicated by DHE (dihydroethidium) fluorescence intensity in the brains of

degradation resulted in small polymer/lipid NCs fragments carrying Mn^{2+} ions which could bound to soluble Aβ in CSF generating higher sensitivity and selectivity. These results indicate that non-invasive MRI of CSF pathology enabled by aAβ-BTRA-NCs can detect definitive signs of an incipient early AD pro-inflammatory process(es) in living subjects.

To verify whether the enhanced MR signal in the CSF is actually reflective of Mn^{2+} ions bound with soluble Aβ and can be correlated with Aβ content in the CSF, direct assay of Mn and Aβ in the CSF is necessary. However, we have found that under the current experimental conditions, it is difficult to collect a sufficient amount of CSF from the Tg mice for the quantitative analysis. Expansion of the scope of this study in larger animal models is thus being pursued to evaluate the applicability of the NCs in clinical translation.

The protection of mouse cortical neurons from oxidative stress and suppression of oxidative stress by Aβ-BTRA-NCs were also investigated. A dose-dependent cytotoxicity study indicated that aAβ-BTRA-NCs were non-toxic to primary cortical neurons up to 50 μM of Mn (Fig. S8a), while H_2O_2 significantly reduced cell viability (Fig. S8b). Introducing aAβ-BTRA-NCs (5 or 15 μM) to neurons treated with 50 μM H_2O_2 raised cell viability by 20 % and 30 %, respectively (Fig. 4j). CLSM showed that 15 μM aAβ-BTRA-NCs did not alter neuronal morphology, instead, protected the neurons from H_2O_2-induced neuronal damage (Fig. 4k). Total cerebral ROS levels before and after NC treatment in Tg and WT mice were measured. The ROS level in untreated Tg mouse brains was 18.7 %, 30 % (1.3-fold) and 60 % (1.6-fold) higher than those in the WT mice at 3-, 6- and 9-month of age, respectively (Fig. 4g). This result supports the hypothesis that higher cerebral ROS (H_2O_2) levels enhance MRI contrast with age by greater production of Mn^{2+} ions in addition to leakier vessels at older ages (Fig. 4b–c). After aAβ-BTRA-NC treatment the cerebral ROS concentrations did not change in WT mice; however, they slightly decreased in 3-month old Tg mice and significantly decreased by 14.9 % and 36.3 % in 6- and 9-month old Tg mice, respectively (Fig. 4g). These results suggest that i.v. injected aAβ-BTRA-NCs selectively attenuate excess ROS; the higher the ROS level, the more profound the effect.

The pro-inflammatory cytokine nterleukin 1 beta (IL-1β) level showed a similar trend of ROS level in relation to mouse age and treatment response. While showing no effect in WT mice and slight effects in 3-month old Tg mice, the aAβ-BTRA-NC treatment reduced cerebral IL-1β concentration by 55 % and 83 % in 6- and 9-month old Tg mice, respectively (Fig. 4h). Interestingly, a 3D-surface plot of normalized CSF MR signals *vs*. ROS and IL-1β levels revealed nearly linear relationships (Fig. 3i), suggesting a novel application of CSF MRI. Based on the MRI signal in the CSF, aAβ-BTRA-NCs could be an effective and quick means for probing ROS and pro-inflammatory cytokine IL-1β level over the different stages of AD. The CSF MRI has the potential to link with clinical biomarkers for an enhanced diagnosis of AD.

Manganese content in WT and Tg mouse brains of various ages was analyzed by ICP-AES 2 h after i.v. injection of aAβ-BTRA-NC. It was found that the WT and 3-month old Tg mice contained similar amounts of cerebral Mn, while the Tg mice at 6- and 9-months of ages showed slightly higher Mn contents (Fig. S9). The relative delivery efficiency of aAβ-BTRA-NCs into the brain of Tg mice, compared to the whole body, 2 h post injection was calculated to be 9.1 %, 10.8 % and 12.0 % in 3-months, 6-months and 9-months old Tg mice, respectively. These results indicate that it is the redox-reaction produced Mn^{2+} instead of total amount of Mn that amplified MR contrast. Taking this finding and the ROS/IL-1β-correlated MR signal together, it can be concluded that the aAβ-BTRA-NC enhanced CSF MR signal is indeed activated by ROS in the brain. The unique functionality of aAβ-BTRA-NCs to respond to ROS and bind with both Aβ and Mn^{2+} gives MRI a useful application in detecting Aβ-induced oxidative stress and inflammation, an early event in AD.

A preliminary assessment of acute toxicity was conducted in 6-month old Tg mice treated with aAβ-BTRA-NCs (100 μmol Mn kg^{-1} of bodyweight). No histological abnormalities in any of the major organs were observed 7 days after the treatment as compared to saline controls (Fig. S10), reducing concerns about the potential toxicity of MnO_2-containing NCs and the production of Mn^{2+} in possible translation to the clinic [48].

Although this work only presents the application of the NC system in an AD model, the application of the NCs can be expanded to brain tumors, strokes, and other neurodegenerative diseases (*e.g.* Parkinson disease, multiple sclerosis). The functional groups (–OH or –COOH) on the BTP can be readily conjugated with corresponding targeting moieties for specific receptors or biomarkers. However, designing such NC systems to achieve desired functionality is challenging and requires specially designed analysis. In addition to full characterization of the chemical structure of the modified polymer and physicochemical properties of the NCs, the multi-stage functionality of the NCs needs to be analyzed. The NCs must first cross the BBB and then expose the disease-specific ligands to the targets in the brain parenchyma. To evaluate such functionality *in vitro*, one may perform a permeation test using an *in vitro* 3D human BBB transwell co-culture assay followed by a binding test on the samples collected from the brain side of the transwell [39] (SI, Fig. S2h). For *in vivo* analysis of BBB penetration and cascade targetability, staining of cell nuclei outside the brain blood microvessles by NP-delivered brain-impermeable dye and microscopic examination of brain sections can offer strong evidence [39,41,42,49] (Figs. 2g–I, 3, SI, S2).

Owing to the complexity and heterogeneity in human subjects, and neuroinflammation found in many CNS diseases, the method presented in this work using targeted-NC with MRI alone may not be able to differentiate among neurodegenerative diseases. Therefore, combining this method with other MRI modes (*e.g.* functional and structural MRI), other imaging modalities, as well as fluid biomarker assays used in clinic is necessary to obtain accurate diagnosis. For further exploration of non-invasive MRI technique as a useful screening and diagnostic means, thorough studies are needed to establish a correlation between targeted NC-MRI and fluid biomarkers (in CSF and blood) pertinent to diseases (*e.g.* Aβ, p-tau, inflammatory cytokines, and neuroinflammation biomarkers).

Conclusions

In summary, we have developed a novel multifunctional and ROS-responsive nanotheranostic system, aAβ-BTRA-NC, and

WT mice and Tg mice of various ages without treatment or at 2 h post i.v. injection of aAβ-BTRA-NCs. **h)** Levels of pro-inflammatory cytokines IL-1β in the brains of WT and Tg mice of different ages without treatment or at 24 h post treatment. The data are presented as mean ± SD (n = 5). **i)** A 3D surface plot of relationships among *in vivo* CSF MRI signal enhancement, *ex vivo* ROS and IL-1β concentrations in brain tissue. All measured values were normalized to WT mice group. **j)** Influence of aAβ-BTRA-NCs on viability of mouse cortical neurons with or without exposed to 50 μm H_2O_2. The data are presented as mean ± SD (n = 3). P values indicate statistically significant difference between aAβ-BTRA-NCs treated groups (**c-e**), or between aAβ-BTRA-NCs treated group and untreated group (**g, h, j**). **k)** Representative CLSM images showing neuronal morphology *in vitro* treated by different groups. WT: wild type; M: month.

demonstrated its ability to enable sensitive detection of early AD by non-invasive MRI of CSF pathology. The aAβ-BTRA-NC effectively crossed the BBB, selectively accumulated in the disease affected areas and significantly enhanced T_1-wt MR signals in the CSF, cortex, hippocampus areas of TgCRND8 AD mouse brains, where overexpressed oxidative stress and Aβ pathology occur. Importantly, the aAβ-BTRA-NCs enhanced CSF MR signals exhibited very high sensitivity (89 %) and specificity (100 %) for disease detection regardless of mouse age and disease severity. The aAβ-BTRA-NCs also showed a potential to protect neurons against H_2O_2-mediated neurotoxicity *in vitro* and attenuate cerebral oxidative stress (ROS and IL-1β) in Tg mice. These results suggest that the multifunctional NC system may serve as a versatile nano-platform for targeted theranostics in early-stage oxidative stress and inflammation-associated acute and chronic neurodegenerative disorders. The present work also encourages further development of such NC system to render MRI a fast and effective screening tool for clinical detection of AD and other neurodegenerative diseases in high risk populations.

Author contributions

X.Y.W, C.H, T.A, J.T.H., and A.Z.A. conceived the hypotheses, designed the experiments, interpreted results, and wrote the paper. C.H, T.A, J.T.H., A.Z.A., L.Y.L, and P.C. performed the experiments. W.D.F. performed the MRI data acquisition and analysis and edited the manuscript. E.K. and P.E.F performed the experiments related to generating TgCRND8 mouse model. P.E.F. and A.M.R. designed the experiments and wrote the paper.

Declaration of Competing Interest

The authors report no declarations of interest.

Acknowledgements

This work is supported by the Weston Brain Institute Transformational Grant to X.Y.W, J.T.H. and P.E.F., University of Toronto Connaught Innovation Award, Killam Research Fellowship by the Canada Council for the Arts, and Equipment Grants from the Natural Sciences and Engineering Research Council of Canada to X.Y.W. The authors also thank the University of Toronto Connaught International Scholarship for Doctoral Students to T.A., the Centre for Collaborative Drug Research Graduate Student Incentive Fund to X.Y.W. and P.E.F., Professor Shana O. Kelley and Dr. Jagotamoy Das (Leslie Dan Faculty of Pharmacy, University of Toronto) for assisting in the measurement of differential pulse voltammetry, the Spatio-Temporal Targeting and Amplification of Radiation Response (STTARR) program and its affiliated funding agencies for providing the imaging facilities.

Appendix A. Supplementary data

Supplementary material related to this article can be found, in the online version, at doi:https://doi.org/10.1016/j.nantod.2020.100965.

References

[1] F. Panza, M. Lozupone, G. Logroscino, B.P. Imbimbo, Nat. Rev. Neurol. 15 (2019) 73–88.
[2] R.M. Anderson, C. Hadjichrysanthou, S. Evans, M.M. Wong, Lancet 390 (2017) 2327–2329.
[3] F. Amirrad, E. Bousoik, K. Shamloo, H. Al-Shiyab, V.V. Nguyen, H. Montazeri Aliabadi, J. Pharm. Pharm. Sci. 20 (2017) 184–225.
[4] D. Mehta, R. Jackson, G. Paul, J. Shi, M. Sabbagh, Expert Opin. Investig. Drugs 26 (2017) 735–739.
[5] H.L. Wong, X.Y. Wu, R. Bendayan, Adv. Drug Deliv. Rev. 64 (2012) 686–700.
[6] L. Robinson, E. Tang, J.-P. Taylor, BMJ 350 (2015) h3029.
[7] B.P. Imbimbo, M. Lozupone, M. Watling, F. Panza, Expert Opin. Investig. Drugs (2020) 1–15, http://dx.doi.org/10.1080/13543784.2020.1795127.
[8] W.A. Banks, Nat. Rev. Drug Discov. 15 (2016) 275–292.
[9] A. Bradford, M.E. Kunik, P. Schulz, S.P. Williams, H. Singh, Alzheimer Dis. Assoc. Disord. 23 (2009) 306–314.
[10] K. Blennow, H. Zetterberg, J. Alzheimers Dis. 62 (2018) 1125–1140.
[11] A.D. Henriques, A.L. Benedet, E.F. Camargos, P. Rosa-Neto, O.T. Nobrega, Exp. Gerontol. (2018).
[12] B. Dubois, H.H. Feldman, C. Jacova, S.T. Dekosky, P. Barberger-Gateau, J. Cummings, A. Delacourte, D. Galasko, S. Gauthier, G. Jicha, K. Meguro, J. O'Brien, F. Pasquier, P. Robert, M. Rossor, S. Salloway, Y. Stern, P.J. Visser, P. Scheltens, Lancet Neurol. 6 (2007) 734–746.
[13] R.J. Bateman, C. Xiong, T.L. Benzinger, A.M. Fagan, A. Goate, N.C. Fox, D.S. Marcus, N.J. Cairns, X. Xie, T.M. Blazey, D.M. Holtzman, A. Santacruz, V. Buckles, A. Oliver, K. Moulder, P.S. Aisen, B. Ghetti, W.E. Klunk, E. McDade, R.N. Martins, C.L. Masters, R. Mayeux, J.M. Ringman, M.N. Rossor, P.R. Schofield, R.A. Sperling, S. Salloway, J.C. Morris, N. Engl. J. Med. 367 (2012) 795–804.
[14] L.K. McEvoy, J.B. Brewer, Expert Rev. Neurother. 10 (2010) 1675–1688.
[15] K.L. Viola, J. Sbarboro, R. Sureka, M. De, M.A. Bicca, J. Wang, S. Vasavada, S. Satpathy, S. Wu, H. Joshi, P.T. Velasco, K. MacRenaris, E.A. Waters, C. Lu, J. Phan, P. Lacor, P. Prasad, V.P. Dravid, W.L. Klein, Nat. Nano 10 (2015) 91–98.
[16] G.B. Frisoni, M. Boccardi, F. Barkhof, K. Blennow, S. Cappa, K. Chiotis, J.F. Démonet, V. Garibotto, P. Giannakopoulos, A. Gietl, O. Hansson, K. Herholz, C.R. Jack Jr., F. Nobili, A. Nordberg, H.M. Snyder, M. Ten Kate, A. Varrone, E. Albanese, S. Becker, P. Bossuyt, M.C. Carrillo, C. Cerami, B. Dubois, V. Gallo, E. Giacobini, G. Gold, S. Hurst, A. Lönneborg, K.O. Lovblad, N. Mattsson, J.L. Molinuevo, A.U. Monsch, U. Mosimann, A. Padovani, A. Picco, C. Porteri, O. Ratib, L. Saint-Aubert, C. Scerri, P. Scheltens, J.M. Schott, I. Sonni, S. Teipel, P. Vineis, P.J. Visser, Y. Yasui, B. Winblad, Lancet Neurol. 16 (2017) 661–676.
[17] K.A. Johnson, N.C. Fox, R.A. Sperling, W.E. Klunk,Cold Spring Harb. Perspect. Med. 2 (2012), a006213.
[18] R. Mistur, L. Mosconi, S.D. Santi, M. Guzman, Y. Li, W. Tsui, M.J. de Leon, J. Clin. Neurol. 5 (2009) 153–166.
[19] G.B. Frisoni, N.C. Fox, C.R. Jack Jr., P. Scheltens, P.M. Thompson, Nat. Rev. Neurol. 6 (2010) 67–77.
[20] H. Rusinek, S. De Santi, D. Frid, W.H. Tsui, C.Y. Tarshish, A. Convit, M.J. de Leon, Radiology 229 (2003) 691–696.
[21] T. den Heijer, M.I. Geerlings, F.E. Hoebeek, A. Hofman, P.J. Koudstaal, M.M. Breteler, Arch. Gen. Psychiatry 63 (2006) 57–62.
[22] A. Weller, J.L. Barber, Ø.E. Olsen, Pediatr. Nephrol. 29 (2014) 1927–1937.
[23] J.A. Rees, G.J. Deblonde, D.D. An, C. Ansoborlo, S.S. Gauny, R.J. Abergel, Sci. Rep. 8 (2018) 4419.
[24] T. Kanda, H. Oba, K. Toyoda, K. Kitajima, S. Furui, J. Radiol. 34 (2016) 3–9.
[25] H.E. Gendelman, V. Anantharam, T. Bronich, S. Ghaisas, H. Jin, A.G. Kanthasamy, X. Liu, J. McMillan, R.L. Mosley, B. Narasimhan, S.K. Mallapragada, Nanomedicine 11 (2015) 751–767.
[26] S. Ding, A.I. Khan, X. Cai, Y. Song, Z. Lyu, D. Du, P. Dutta, Y. Lin, Mater. Today (2020).
[27] M. Rosini, E. Simoni, A. Milelli, A. Minarini, C. Melchiorre, J. Med. Chem. 57 (2014) 2821–2831.
[28] S. Chakrabarti, M. Sinha, I.G. Thakurta, P. Banerjee, M. Chattopadhyay, Curr. Med. Chem. 20 (2013) 4648–4664.
[29] T. Chitnis, H.L. Weiner, J. Clin. Invest. 127 (2017) 3577–3587.
[30] M.T. Heneka, M.J. Carson, J. El Khoury, G.E. Landreth, F. Brosseron, D.L. Feinstein, A.H. Jacobs, T. Wyss-Coray, J. Vitorica, R.M. Ransohoff, K. Herrup, S.A. Frautschy, B. Finsen, G.C. Brown, A. Verkhratsky, K. Yamanaka, J. Koistinaho, E. Latz, A. Halle, G.C. Petzold, T. Town, D. Morgan, M.L. Shinohara, V.H. Perry, C. Holmes, N.G. Bazan, D.J. Brooks, S. Hunot, B. Joseph, N. Deigendesch, O. Garaschuk, E. Boddeke, C.A. Dinarello, J.C. Breitner, G.M. Cole, D.T. Golenbock, M.P. Kummer, Lancet Neurol. 14 (2015) 388–405.
[31] J. Cummings, G. Lee, A. Ritter, M. Sabbagh, K. Zhong, Alzheimers Dement (N Y) 5 (2019) 272–293.
[32] T. Persson, B.O. Popescu, A. Cedazo-Minguez, Oxid. Med. Cell. Longev. 2014 (2014) 11.
[33] C.R. Gordijo, A.Z. Abbasi, M.A. Amini, H.Y. Lip, A. Maeda, P. Cai, P.J. O'Brien, R.S. DaCosta, A.M. Rauth, X.Y. Wu, Adv. Funct. Mater. 25 (2015) 1858–1872.
[34] P. Prasad, C.R. Gordijo, A.Z. Abbasi, A. Maeda, A. Ip, A.M. Rauth, R.S. DaCosta, X.Y. Wu, ACS Nano 8 (2014) 3202–3212.
[35] J. Li, P. Cai, A. Shalviri, J.T. Henderson, C. He, W.D. Foltz, P. Prasad, P.M. Brodersen, Y. Chen, R. DaCosta, A.M. Rauth, X.Y. Wu, ACS Nano 8 (2014) 9925–9940.
[36] D. Wu, M. Qin, D. Xu, L. Wang, C. Liu, J. Ren, G. Zhou, C. Chen, F. Yang, Y. Li, Y. Zhao, R. Huang, S. Pourtaheri, C. Kang, M. Kamata, I.S.Y. Chen, Z. He, J. Wen, W. Chen, Y. Lu,Adv. Mater. 31 (2019), 1807557.
[37] M. Nowak, M.E. Helgeson, S. Mitragotri,Adv. Ther. 3 (2020), 1900073.
[38] G. Tosi, J.T. Duskey, J. Kreuter, Expert Opin. Drug Deliv. 17 (2020) 23–32.
[39] H. Chunsheng, L. Jason, C. Ping, A. Taksim, H.J. T, F.W. D, B. Reina, R.A. Michael, W.X. Yu,Adv. Funct. Mater. 28 (2018), 1705668.
[40] B. Wilson, M.K. Samanta, K. Santhi, K.P. Kumar, N. Paramakrishnan, B. Suresh, Eur. J. Pharm. Biopharm. 70 (2008) 75–84.
[41] C. He, P. Cai, J. Li, T. Zhang, L. Lin, A.Z. Abbasi, J.T. Henderson, A.M. Rauth, X.Y. Wu, J. Control. Release 246 (2017) 98–109.

[42] J. Li, P. Cai, A. Shalviri, J.T. Henderson, C. He, W.D. Foltz, P. Prasad, P.M. Brodersen, Y. Chen, R. DaCosta, A.M. Rauth, X.Y. Wu, ACS Nano 8 (2014) 9925–9940.
[43] J. Kreuter, D. Shamenkov, V. Petrov, P. Ramge, K. Cychutek, C. Koch-Brandt, R. Alyautdin, J. Drug Target 10 (2002) 317–325.
[44] S. Wohlfart, S. Gelperina, J. Kreuter, J. Control. Release 161 (2012) 264–273.
[45] C. Janus, J. Pearson, J. McLaurin, P.M. Mathews, Y. Jiang, S.D. Schmidt, M.A. Chishti, P. Horne, D. Heslin, J. French, H.T. Mount, R.A. Nixon, M. Mercken, C. Bergeron, P.E. Fraser, P. St George-Hyslop, D. Westaway, Nature 408 (2000) 979–982.
[46] M.A. Chishti, D.S. Yang, C. Janus, A.L. Phinney, P. Horne, J. Pearson, R. Strome, N. Zuker, J. Loukides, J. French, S. Turner, G. Lozza, M. Grilli, S. Kunicki, C. Morissette, J. Paquette, F. Gervais, C. Bergeron, P.E. Fraser, G.A. Carlson, P.S. George-Hyslop, D. Westaway, J. Biol. Chem. 276 (2001) 21562–21570.
[47] L.M. Shaw, M. Korecka, C.M. Clark, V.M. Lee, J.Q. Trojanowski, Nat. Rev. Drug Discov. 6 (2007) 295–303.
[48] X. Feng, A. Chen, Y. Zhang, J. Wang, L. Shao, L. Wei, Int. J. Nanomed. 10 (2015) 4321–4340.
[49] T. Zhang, H. Lip, C. He, P. Cai, Z. Wang, J.T. Henderson, A.M. Rauth, X.Y. Wu,Adv. Healthc. Mater. 8 (2019), e1900543.

Dr. Chunsheng He received his PhD degree on Chemo-Biological Technology and Engineering from the East China University of Science and Technology, Shanghai, China. He then worked at the University of Toronto as a postdoctoral fellow from 2012 to 2017. After that, he works as a Research Associate and project leader in Dr. Xiao Yu Wu's lab, University of Toronto. His research focuses on the development of novel polymer-lipid based nano formulations for targeting and locoregional delivery of anticancer drugs, polypeptides, proteins, antibodies, and hybrid MnO_2 nanoparticles for the treatment and diagnosis of cancer and central nervous system diseases.

Taksim Ahmed is a PhD Candidate under the supervision of Professor Wu at the University of Toronto. He received B. Pharmacy degree from Jahangirnagar University, Bangladesh in 2009. Afterwards, he worked in ACI Pharmaceuticals LTD, Bangladesh (2009−10). He received his Master's in Pharmacy degree from the College of Pharmacy, Chosun University, S. Korea (2012) and second M.Sc. degree at the School of Pharmacy, University of Waterloo, Canada (2015). He is a recipient of Connaught International Scholarship for Doctoral Students. His current research is focused on developing nanoparticulate drug delivery systems for the treatment of cancer and central nervous system diseases.

Dr. Azhar Z. Abbasi received Master's degree from Quaid-i-Azam University, Pakistan, in 2006 and Ph.D. degree from Philipps-Universität Marburg, Germany, in 2010. In 2011, he joined Professor Wu at University of Toronto as a Postdoctoral fellow. In 2016, Dr. Abbasi joined pharmaceutical company, Apotex Inc., and worked in Research and Development Department for two years. Currently, he is working as a Research associate and Project leader at Faculty of Pharmacy, University of Toronto. His current research focuses on development of biocompatible and multifunctional polymer/lipid nanoparticle formulations, for drug delivery, imaging and diagnostic of cancer and central nervous system (CNS) diseases.

Lily Yi Li is a Ph.D. student in the laboratory of Professor X.Y. Wu at the University of Toronto. She received her B.Sc. degree (2015) in Pharmaceutical Chemistry and M.Sc. degree (2017) in Pharmaceutical Sciences from University of Toronto, Canada. She started doing research since 2nd year of her undergraduate program, then joined the current lab for her studies. Her research interests include Alzheimer's research, oncology research, developing and synthesizing bio-environmental responsive and targeting nanomaterials and intelligent drug delivery systems, as well as mathematical modeling and computational simulation for mechanistic studies on drug delivery.

Dr. Warren D. Foltz is the MRI physicist at the STTARR Innovation Centre, where he operates and consults on MRI projects using a 7 T Biospec (Bruker Corporation) and 1.5 T Aera (Siemens Corporation). He has broad experience across quantitative MRI applications, field strengths, nanoparticles, and animal and disease models. He is currently an Assistant Professor in the Faculty of Radiation Oncology of the University Health Network and University of Toronto. He received his Ph.D. from Medical Biophysics at the University of Toronto.

Dr. Ping Cai received his MD and MSc degrees in Medicine in China, conducted postdoctoral research in toxicology at UTMB (TX, US) and in drug toxicity at the University of Toronto, Canada. He has worked in Dr. Wu's laboratory as a Research Associate since 2011. His research work includes development of animal models of primary tumors and cancer metastases in the lungs and brain, CNS diseases, in vivo studies of toxicity, efficacy, and immune modulation of nanomedicine.

fx**7Dr. Erin Knock** received her PhD degree, in 2009, from McGill University. She then worked at the University of Cambridge as a postdoctoral scholar from 2009 to 2012. After that, she worked at the University of Toronto as a post-doc from 2012 to 2016 on the development of human stem cell-derived neuronal models of Alzheimer's Disease. In 2016, Dr. Knock joined the Research and Development Department at STEMCELL Technologies Inc. as a Senior Scientist. Dr Knock's current research focuses on developing products for primary neural culture and pluripotent stem cell differentiation to neural cell types.

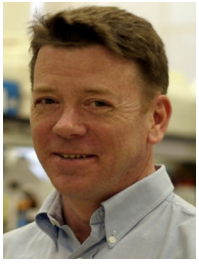

Dr. Paul E. Fraser is a full professor in the Departments of Medical Biophysics at the University of Toronto and Jeno Diener Chair in Neurodegenerative Diseases, Tanz Centre, Canada. His group has been examining the organization and mechanisms by which amyloid-β (Aβ) peptides are assembled into oligomeric and fibrillar structures in Alzheimer disease (AD). Research is also being conducted into the unique family of presenilin proteins since their discovery at the Tanz Centre, and the investigations have been expanded to determine the mechanisms of action for groups of AD at-risk genes identified by genome-wide association studies.

Dr. Andrew M. Rauth is an Emeritus Professor in the Departments of Medical Biophysics and Radiation Oncology at the University of Toronto and Scientist Emeritus at Princess Margaret Cancer Centre, University Health Network Toronto, Ontario, Canada. Research interests are radiation biology, mechanisms of drug action and nanoparticles. He has been a collaborator of Dr. Wu for over 20 years.

Dr. Jeffrey T. Henderson is an Associate Professor in the Faculty of Pharmacy, University of Toronto. He received his Ph.D. in Biochemistry at University of Illinois, Chicago. Following postdoctoral work in the Divisions of Development and Neuroscience, and Molecular Biology and Cancer at the Samuel Lunenfeld Research Institute Mount Sinai Hospital he became an Assistant Scientist at SLRI in Molecular Neuroscience. His laboratory focuses on mechanisms of natural and neuropathologic cell death signaling within the mammalian CNS with the aim of developing small molecular PCD neurotherapeutics. He joined the Faculty of Pharmacy, University of Toronto in 2002.

Dr. Xiao Yu Wu is full professor at the Leslie Dan Faculty of Pharmacy at the University of Toronto, Canada. She received her Ph.D. degree in Chemical Engineering from McMaster University, Canada. After postdoctoral research at the University of Toronto, she joined the Faculty of Pharmacy in 1994. Her research projects are centered on advanced pharmaceutics and drug delivery technologies including blood-brain barrier penetrating nanoparticles for brain cancer and CNS diseases; synergistic drug combination nanomedicine for enhanced chemotherapy; hybrid MnO2 nanoparticles for enhancing cancer therapies and theranostics of Alzheimer's disease; computer-aided design of controlled release dosage forms; glucose-responsive insulin/glucagon delivery.